ACS APPLIED MATERIALS & INTERFACES

Research Article

www.acsami.org

Conjugated Polymer-Based Hybrid Nanoparticles with Two-Photon Excitation and Near-Infrared Emission Features for Fluorescence Bioimaging within the Biological Window

Yanlin Lv,[†] Peng Liu,[‡] Hui Ding,[†] Yishi Wu,[§] Yongli Yan,[§] Heng Liu,[†] Xuefei Wang,[†] Fei Huang,*[,‡] Yongsheng Zhao,*[,§] and Zhiyuan Tian*[,†]

[†]School of Chemistry and Chemical Engineering, University of Chinese Academy of Sciences (UCAS), Beijing 100049, China

[‡]Institute of Polymer Optoelectronic Materials & Devices, State Key Laboratory of Luminescent Materials & Devices, South China University of Technology, Guangzhou, 510640, China

[§]Beijing National Laboratory for Molecular Science (BNLMS) and Key Laboratory for Photochemistry, Institute of Chemistry Chinese Academy of Sciences, Beijing, 100190, China

ABSTRACT: Hybrid fluorescent nanoparticles (NPs) capable of fluorescing near-infrared (NIR) light (centered ~730 nm) upon excitation of 800 nm laser light were constructed. A new type of conjugated polymer with two-photon excited fluorescence (TPEF) feature, P-F8-DPSB, was used as the NIR-light harvesting component and the energy donor while a NIR fluorescent dye, DPA-PR-PDI, was used as the energy acceptor and the NIR-light emitting component for the construction of the fluorescent NPs. The hybrid NPs possess δ value up to 2.3×10^6 GM per particle upon excitation of 800 nm pulse laser. The excellent two-photon absorption (TPA) property of the conjugated polymer component, together with its high fluorescence quantum yield (ϕ) up to 45% and the efficient energy transfer from the conjugated polymer to NIR-emitting fluorophore with efficiency up to 90%, imparted the hybrid NPs with TPEF-based NIR-input-NIR-output fluorescence imaging ability with penetration depth up to 1200 μm. The practicability of the hybrid NPs for fluorescence imaging in Hela cells was validated.

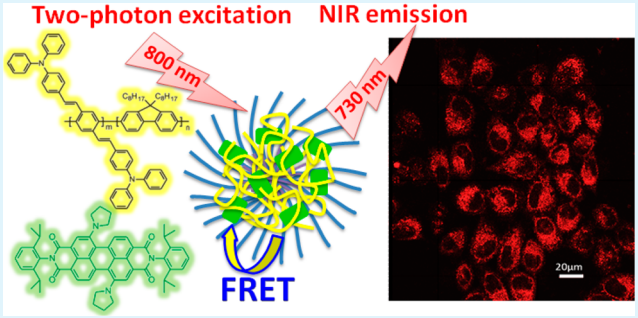

KEYWORDS: *two-photon absorption, near-infrared (NIR) fluorescence, multiphoton fluorescence bioimaging, energy transfer, conjugated polymer*

INTRODUCTION

Fluorescence bioimaging is characterized by its ability of inherently enabling the noninvasive studies of gene, protein, and cellular processes with single-molecule sensitivity, excellent spatiotemporal resolution, and ease of manipulation.[1−4] Such feature makes fluorescence imaging a versatile modality for direct visualization of physiological processes in living organisms, probing biological structures, and exploring information regarding various biological mechanisms.[5−8] The key enabling technology is the fluorescent probes with optimized properties. However, most conventional fluorescent probes are generally excited via UV or visible light and therefore suffer from the limited penetration depth of excitation light in imaging deep-seated target and thick samples.[9,10] Because of the maximum optical transparency of many tissues in the biological window (~700−1000 nm),[11] introduction of fluorescent probes with two- (or multi-)photon excited fluorescence (TPEF or MPEF) emission feature and can be excited by the laser light with near-infrared (NIR) wavelengths has been proved an effective strategy to circumvent such impediment of penetration depth.[9,12,13] Additionally, because of the relatively low two-photon absorption (TPA) ability of most native biomolecules in the biological window and the quadratic dependence of TPA on the excitation laser power, TPA-based excitation using NIR light can markedly reduce background signal arising from autofluorescence and enable highly localized excitation, which effectively facilitates biological imaging with enhanced resolution.[8,14−16]

It deserves mentioning that absorption and light scattering caused by cellular structures and tissues are detrimental to both incoming (excitation) and outgoing (emission) light. Specifically, optical loss of the incoming light is generally responsible for the limited penetration depth of excitation light while attenuation of the outgoing light results in the reduced fluorescence signal and discrimination of signal from the background.[17,18] Ultimately, ideal fluorescence bioimaging demands the probes to possess TPEF emission feature with excitation and emission both in the NIR region. Considerable of progress have been achieved in the TPEF-based[19−22] and the

Received: June 11, 2015
Accepted: September 4, 2015
Published: September 4, 2015

DOI: 10.1021/acsami.5b05150
ACS Appl. Mater. Interfaces 2015, 7, 20640−20648

Scheme 1. Chemical Structures of the Conjugated Polymer with TPEF Feature (P-F8-DPSB), NIR Fluorescent Dye (DPA-PR-PDI), the Amphiphilic Tri-block Polymer with Grafted Folate Moiety (FA-F127) Used for the Construction of the Hybrid NPs, and Illustration Showing the NIR Fluorescence Emission of the NPs upon TPA-Based Excitation Using 800 nm Pulse Laser

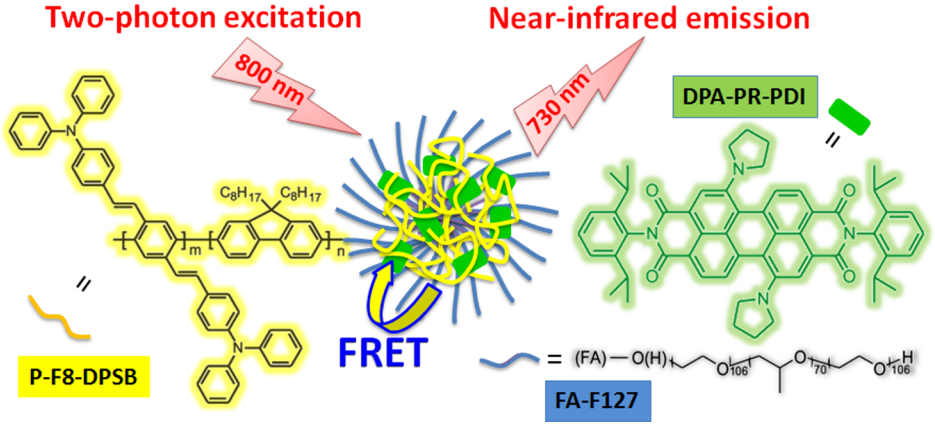

Scheme 2. Synthetic Routes for the Target Conjugated Polymer P-F8-DPSB

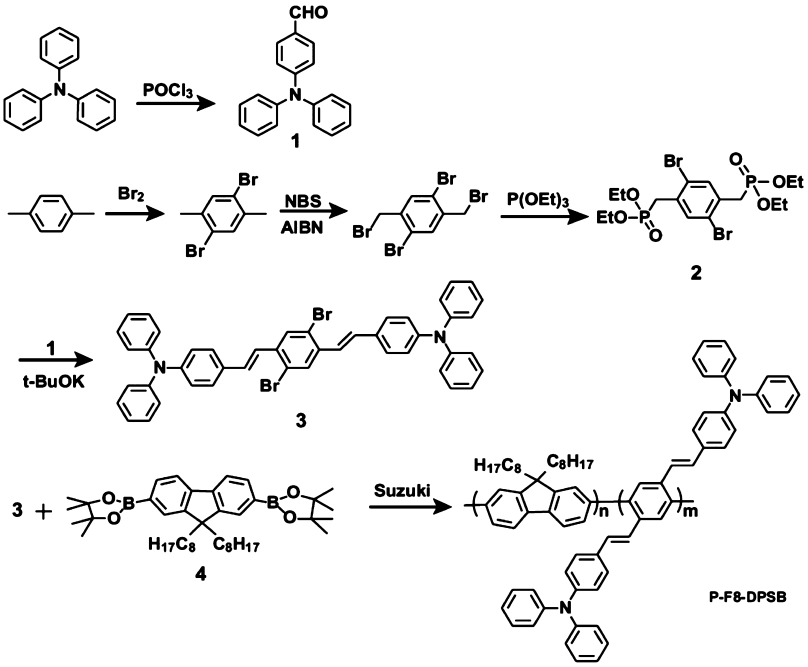

NIR-based biological fluorescence imaging.[23−25] However, fluorescent probe possessing TPEF ability with excitation and emission wavelengths both in NIR region has rarely been reported thus far. In the present work, we developed a new type of fluorescent probes capable of emitting NIR fluorescence (centered ~730 nm) upon excitation of 800 nm pulse laser based on the combination of TPEF and Förster resonance energy transfer (FRET) mechanism (Scheme 1). Owing to such salient property of NIR-incoming-NIR-outgoing, this type of probes displayed superior ability for imaging thick samples as compared to the conventional fluorescent probes with excitation and emission in visible region. Additionally, these fluorescent probes were functionalized with targeting moieties, folate (FA), for selective recognition of the target cancer cells because of the preferential binding of FA to the FA receptor that was highly expressed on the surfaces of cancer cells. Such feature of merits of these probes, together with the validation of their biocompatibility and intracellular fluorescence imaging ability, are indicative of their potential for fluorescence bioimaging for deep-seated target and thick samples.

EXPERIMENTAL SECTION

Materials. Pluronic nonionic surfactant, poly(ethylene oxide)-*b*-poly(propylene oxide)-*b*-poly(ethylene oxide), Pluronic F127 (M_w = 12 600) was purchased from Sigma-Aldrich. Milli-Q water with a resistivity of 18.2 MΩ·cm^{-1}, produced using a Milli-Q apparatus (Millipore), was used in all experiments. All other chemicals were purchased from J & K Scientific, Ltd., and used without further purification.

Synthesis of Conjugated Polymer P-F8-DPSB.[26] 4-(Diphenylamino)benzaldehyde (**1**), 2,5-bis(diethyl phosphonatomethyl)-1,4-dibromobenzene (**2**), and 2, 7-bis (4, 4, 5, 5-tetramethyl-1, 3, 2-dioxaborolan-2-yl)-9, 9-dioctylfluorene (**3**) were synthesized according to the previously reported strategies (Scheme 2). 2,7-bis(4,4,5,5-tetramethyl-1,3,2-dioxaborolan-2-yl)-9,9-dioctylfluorene (**4**) was prepared following the reported procedures.[27] Compound **2** (2.68 g, 5 mmol) was added to a solution of potassium *tert*-butoxide (1.68 g, 15 mmol) in dry THF (15 mL) at 0 °C and then the mixture was stirred for

DOI: 10.1021/acsami.5b05150
ACS Appl. Mater. Interfaces 2015, 7, 20640−20648

1 h. A solution of compound 1 (3.00 g, 11 mmol) in dry THF was added via syringe and the resulting mixture was then stirred at room temperature for 12 h. The reaction mixture was poured into water and extracted with CH_2Cl_2. The organic layer was washed with water, dried $MgSO_4$, and concentrated under reduced pressure, recrystallization (CH_2Cl_2/ hexane) afforded compound **3** as yellow solid (2.01 g, 52%). ^{1}H NMR (300 MHz, $CDCl_3$): δ 7.83 (s, 2H), 7.41 (d, 4H), 7.28 (t, 4H), 7.26 (d, 4H), 7.24 (d, 2H), 7.13 (d, 8H), 7.06 (m, 8H), 7.00 (d, 2H). ^{13}C NMR (300 MHz, $CDCl_3$): δ 148.30, 147.55, 137.44, 131.71, 130.71, 130.20, 129.54, 128.05, 124.98, 124.08, 123.53, 123.24, 123.07. MS (APCI, m/z): calcd. for $C_{46}H_{34}Br_2N_2$ $[M + 1]^+$ 773.11; found 772.12.

Compound **3** (160.6 mg, 0.25 mmol), compound **4** (193.6 mg, 0.25 mmol), and $Pd(PPh_3)_4$ (10 mg) were dissolved in toluene (5 mL). An aqueous K_2CO_3 solution (2 M, 2 mL) was added to the mixture under nitrogen atmosphere and the reaction mixture was degassed. The mixture was stirred at 85 °C for 24 h under nitrogen atmosphere. The reaction mixture was cooled to room temperature and poured into methanol (200 mL) to precipitate the resulting polymer. The resulting solid was filtered and dissolved in chloroform (20 mL). The solution was washed with water (300 mL) several times. The organic phase was separated and concentrated in vacuo to obtain the product in solid state, which was then purified by Soxhlet extraction with acetone. The polymer was extracted with chloroform followed by silica-gel chromatography with chloroform eluent. The polymer was reprecipitated using methanol and dried in vacuum at 60 °C overnight. Finally, the polymer was obtained as yellow solid (yield = 85%). GPC: M_n= 54.4 kDa, M_w = 131.7 kDa, PDI = 2.41.

Synthesis of NIR-Emitting Dye DPA-PR-PDI.[28] 1,7-Dibromoperylene-3,4,9,10-tetracarboxydianhydride (1.06 g, 1.93 mmol) and 2,6-diisopropylaniline (3.64 mL, 19.3 mmol) were added to a two-neck bottle, and then added ~10 mL propionic acid. The reaction mixture was refluxed overnight. The reaction system was cooled to room temperature. A precipitate formed and was filtered off, washed with propionic acid, ethyl alcohol and water three times under suction, until the filtrate was shallow. The red crude product was then purified by column chromatography on silica gel with a dichloromethane/ chloroform (1:1) solvent mixture. Yield: 554.9 mg (33%) as a red solid. ^{1}H NMR (400 MHz, $CDCl_3$): δ 9.56 (d, J = 8.1 Hz, 2H), 9.02 (s, 2H), 8.81 (d, J = 8.1 Hz, 2H), 7.52 (t, J = 7.8 Hz, 2H), 7.37 (d, J = 7.8 Hz, 4H), 2.77−2.70 (m, 4H), 1.19 (d, J = 6.8 Hz, 24H). ^{13}C NMR (100 MHz, $CDCl_3$): δ 163.2, 162.7, 145.8, 138.6, 133.6, 133.4, 130.8, 130.3, 130.0, 129.8, 128.9, 127.9, 124.4, 123.4, 123.0, 121.2, 53.6, 29.5, 24.2. MS (MALDI-TOF, m/z): calcd. for $C_{48}H_{40}Br_2N_2O_4$ 868.13; found 891.3 $[M + Na]^+$.

A solution of the product in the above step (554.9 mg, 0.64 mmol) in pyrrolidine (15 mL) was heated at 55 °C (external temperature) with an oil bath for 14 h. The unreacted pyrrolidine was slowly neutralized by 10% hydrochloric acid under ice water bath and stirred for 5 h. The resulting mixture was poured into a biphasic mixture of dichloromethane (100 mL) and water (50 mL). After extraction and chromatography column chromatography on silica gel, the precipitation from eluent gave DPA−PR-PDI (323.5 mg, 0.38 mmol, 60% yield) as green solids. ^{1}H NMR (600 MHz, $CDCl_3$): δ 8.51 (d, J = 7.9 Hz, 2H), 7.78 (d, J = 7.9 Hz, 2H), 7.48 (d, J = 7.7 Hz, 2H), 7.35 (t, J = 7.8 Hz, 6H), 3.88−3.81 (m, 8H), 2.97−2.85 (m, 4H), 1.73 (q, J = 7.1 Hz, 8H), 1.18 (q, J = 6.8 Hz, 24H). ^{13}C NMR (150 MHz, $CDCl_3$): δ 164.3, 146.8, 145.8, 134.9, 131.3, 130.6, 129.5, 127.3, 124.0, 123.0, 122.1, 121.4, 119.3, 118.5, 68.0, 67.8, 52.5, 29.1, 26.0, 24.1, 24.0. MS (MALDI-TOF, m/z): calcd. for $C_{56}H_{56}N_4O_4$ 848.43; found 871.6 $[M + Na]^+$.

Synthesis of the folate-grafted Pluronic F127 (FA-F127). The folate moiety was grafted on the Pluronic F127 via the esterification reaction.[29] Folate (11 mg, 0.025 mmol) was dissolved in 15 mL of dry dimethyl sulfoxide (DMSO), and then dicyclohexylcarbodiimide (DCC) (5.3 mg, 0.025 mmol) and 4-dimethylaminopyridine (DMAP) (3 mg, 0.025 mmol) were added with vigorous stirring for 1 h at room temperature. The Pluronic F127 was sonicated in 5 mL of DMSO and subsequently dropwise added into the activated folic acid solution. The reaction mixture was stirred at room temperature for 5 days and followed by dialysis (MWCO = 1000 Da) for an additional 2 days to remove unconjugated folic acid and DMSO. The final aqueous solution was freeze-dried to form pale yellow powder. The structure of the folate grafted Pluronic F127 was confirmed by FT-IR and MALDI-TOF.

Preparation of P-F8-DPSB/DPA-PR-PDI NPs. The target hybrid NPs were prepared via the coprecipitation method reported previously.[2,25] In a typical protocol, 1 mL of homogeneous solution of P-F8-DPSB, DPA-PR-PDI, and FA-F127 in THF was rapidly injected into 10 mL of deionized water under brief sonication. The THF was removed by partial vacuum evaporation and the resulting NPs suspension was filtered through a 220 nm membrane filter (Millipore) to remove larger aggregates, giving clear bright aqueous NPs dispersion. The ratio of P-F8-DPSB to DPA-PR-PDI in the NPs was tuned by changing the feeding ratio of these two components.

Instruments and Characterization Methods. The structures of the conjugated polymer with TPEF features, poly[(9,9-di-*n*-octylfluorene-2,7-diyl)-*alt*-co-(2,5-bis(4-(*N*,*N*-(diphenylmino)styryl) benzene)-1,4-diyl)] (P-F8-DPSB), and the perylenediimide (PDI) derivative dye, DPA-PR-PDI, were characterized by nuclear magnetic resonance spectroscopy (NMR). The structure of folic acid grafted Pluronic F127 was confirmed via transmission mode on a Fourier-transform infrared spectrophotometer (FT-IR, American Nicolet Corp. Model 170-SX). The hydrated diameter of the NPs was measured by dynamic light scattering (DLS) (Zetasizer Nano ZS, Malvern). UV−vis absorption spectra were recorded on Shimadzu UV2550 UV−vis Spectrophotometers. Fluorescence emission spectra were acquired on Horiba FluoroMax4 Spectrofluometer. The relative fluorescence quantum yields of the solution and nanoparticle samples were determined using rhodamine B as a reference (ϕ = 0.70).

For TPEF spectra collection experiments, the excitation light came directly from the fundamental (800 nm, 120 fs, 1 kHz) of the regenerative amplifier (Spitfire, Spectra Physics) seeded with a mode-locked Ti:sapphire laser (Tsunami, Spectra Physics) with the excitation power adjusted by using a set of neutral density filters. TPA cross sections were evaluated via a comparative method, by measuring the TPEF using Rhodamine B as a reference compound. The fundamental of a mode-locked Ti:sapphire laser (770−830 nm, Tsunami) was focused into a lidded quartz cuvette, and detected with a charge-coupled device (CCD) cooled by liquid nitrogen (SPEC-10-400 B/LbN, Roper Scientific) attached to a polychromator (Spectropro-550i, Acton).[30]

The cytotoxicity of the as-prepared P-F8-DPSB/DPA-PR-PDI NPs was evaluated using a CCK-8 assays. HeLa cells were cultured in a full culture medium DMEM containing various concentrations of P-F8-DPSB/DPA-PR-PDI NPs encapsulated with F127 and FA-F127, respectively, for 12 h at 37 °C in an atmosphere of 5% CO_2. The CCK-8 reagent was added and the HeLa cells were incubated at 37 °C for another 2 h. The cell viability was determined by an ELISA microplate reader.

The imaging depth of the P-F8-DPSB/DPA-PR-PDI NPs was investigated using a laser confocal scanning fluorescence microscope with the excitation wavelength of 405 nm and a multiphoton fluorescence microscope with the excitation wavelength of 800 nm. Intralipid was used as the simulated tissue phantom for its turbidity and scattering properties similar to those of the real tissue. To set up intralipid-based simulated tissue phantom with different thickness, two coverslips were stacked face-to-face and two strips of double-sided adhesive with different layers were intercalated between both ends of the coverslips, which creates a gap between the coverslips with different heights. Filling up such gap with 1% intralipid creates the target simulated tissue phantom with specific thickness. The fluorescence images of different tissue phantom thickness were acquired via tuning the number of layer of the double-sided adhesive intercalated between the two coverslips.

The TPEF-based biological imaging was carried out with a multiphoton fluorescence microscope. HeLa cells were grown in DMEM supplemented with 10% (v/v) FBS, 100 U/mL of penicillin, and 100 U/mL of streptomycin.[31] Before the imaging, HeLa cells were incubated with Pluronic F127 and folic acid grafted Pluronic F127 encapsulated P-F8-DPSB/DPA-PR-PDI NPs, respectively, at 37 °C for 2h. The HeLa cells were immobilized with dilute formaldehyde solution before imaging. For the TPEF-based simulated deep-tissue cell imaging,

DOI: 10.1021/acsami.5b05150
ACS Appl. Mater. Interfaces 2015, 7, 20640−20648

Scheme 3. Synthetic Routes for the NIR Fluorescent Dye DPA-PR-PDI and FA-Functionalized Amphiphilic Triblock Copolymer FA-F127

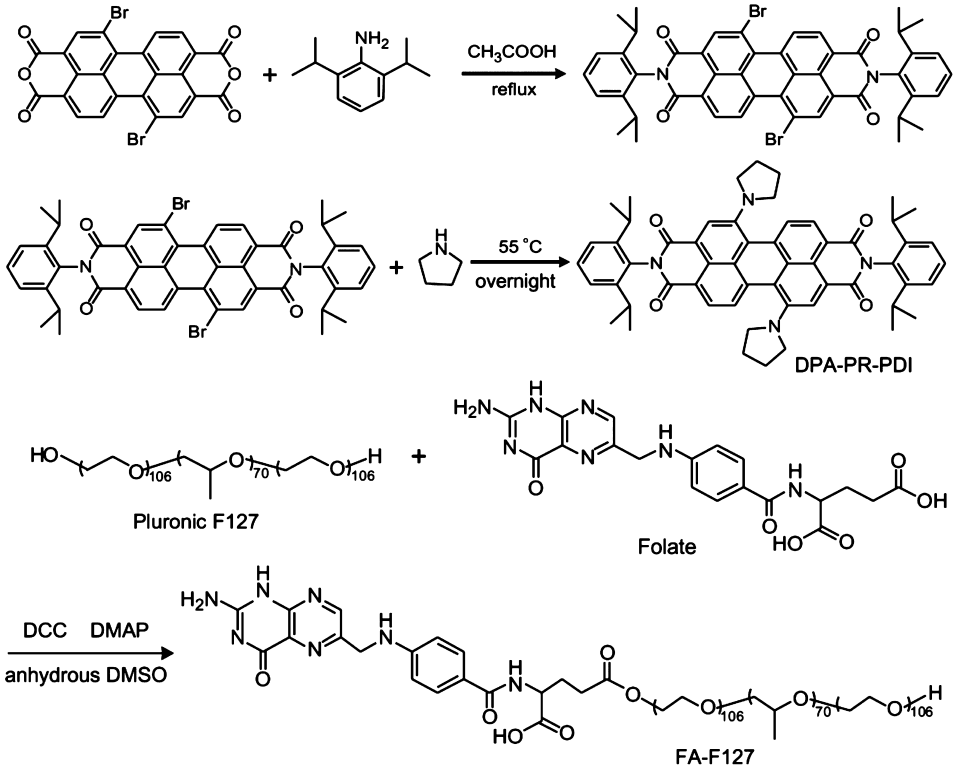

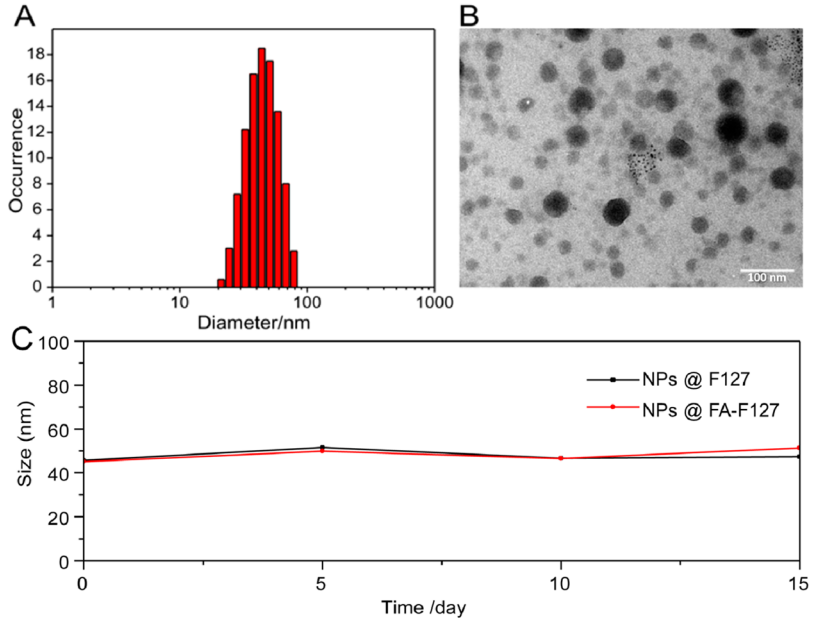

Figure 1. (A) DLS measurement of the as-prepared hybrid NPs. (B) Representative TEM image of the same batch of hybrid NPs. (C) Evolution of hydrodynamic diameter of the F127/FA-F127 encapsulated hybrid NPs in PBS buffer with storing time up to 15 days.

HeLa cells were treated following the similar procedure and 1% intralipid was filled up into the gap with height of 900 μm between the cell culture dish and the coverslip as the simulated tissue phantom, similar to the aforementioned procedure.

RESULTS AND DISCUSSION

Bis(diphenylaminostyryl)benzene (DPSB)-based chromophores are characterized by their large TPA cross section (δ) owing to their typical donor-π-donor (D-π-D) structure.[32] In the present work, a type of DPSB-based conjugated polymer (P-F8-DPSB) was synthesized according to the literatures[26] and used as the two-photon harvesting components and energy donor for construction of the target NPs. A type of fluorescent dye with NIR fluorescence emission feature, a peryleneimide derivative with two strong electron-donating pyrrolidine moieties at the perylene core and two bulky 2,6-diisopropylphenyl moieties at both imide ends (DPA-PR-PDI), was synthesized and used as the

DOI: 10.1021/acsami.5b05150
ACS Appl. Mater. Interfaces 2015, 7, 20640−20648

energy acceptor (Scheme 3). Peryleneimide-based dyes are characterized by their chemo-, thermo-, and photostability. Specifically, introduction of strong electron-donating pyrrolidine moieties at the perylene core enables strong absorption and fluorescence emission in the NIR region, while the presence of the bulky substituent at the imide nitrogen is expected to alleviate the aggregation of the dye and fluorescence self-quenching. Folic acid (FA) moiety was grafted on the amphiphilic triblock copolymer Pluronic F127 via the esterification strategy and the obtained FA-functionalized polymer (FA-F127) was used to decorate the surfaces of the target NPs to impart them with targeting features.

The target hybrid NPs containing the TPEF component P-F8-DPSB, the NIR-emitting component DPA-PR-PDI, and FA-functionalized amphiphilic triblock copolymer FA-F127 were fabricated via a coprecipitation strategy. Owing to the miscibility of THF with water and the insolubility of highly hydrophobic P-F8-DPSB in water, the sudden change of solvent quality upon mixing induces the collapse and aggregation of P-F8-DPSB polymer chains, forming polymer NPs. For the DPA-PR-PDI molecules, their highly hydrophobic characteristics also drive them to aggregate in water, and the hydrophobic interactions between P-F8-DPSB components and DPA-PR-PDI are expected to lead to the formation of NPs with the DPA-PR-PDI more or less evenly incorporated throughout the NPs. Amphiphilic F-127 copolymer has a hydrophobic segment poly(propylene oxide) (PPO) sandwiched between hydrophilic poly(ethylene oxide) (PEO) segments. During the change of solvent quality, the PPO segments are expected to entwine with the hydrophobic P-F8-DPSB polymer chains due to hydrophobic interactions while the PEO segments extended into the aqueous phase. As a result, hybrid NPs with two photoactive components, P-F8-DPSB and DPA-PR-PDI, residing in the hydrophobic core and the FA-containing hydrophilic F-127 segments decorating on the surfaces were constructed, as illustrated in Scheme 1.

Figure 1 displays the dynamic light scattering (DLS) and transmission electron microscope (TEM) characterization results of a representative batch of the as-prepared hybrid P-F8-DPSB/DPA-PR-PDI NPs. DLS measurement result reports an average hydrodynamic radius of ∼45 nm and a relatively narrow polydispersity, while the TEM characterization of the same NPs sample reveals their spherical shape with diameter roughly consistent with the DLS measurement results. Additionally, the NPs aqueous dispersion sample shows a zeta potential of −40.5 mV, indicating a good stability of the as-prepared hybrid NPs sample. As compared to the freshly prepared NPs sample, NPs in PBS stored 15 days did not display noticeable changes in the hydrodynamic radius, which verifies the size stability of the hybrid NPs investigated in the present work (Figure 1C). Moreover, fluorescence quantum yield of the NPs stored 2 weeks was found similar to that of fresh NPs sample, suggesting no noticeable leaching of the dye from the NPs occurred. This result is in agreement with previously reported results regarding the structural stability of conjugated polymer NPs with incorporated hydrophobic small-molecular-weight dyes and dopants.[33,34]

For the practical application of TPEF-based imaging, the selection of the appropriate probes is impeded by the TPA cross section (δ) of most of the commonly used fluorophores. To evaluate the TPA performance of P-F8-DPSB conjugated polymer within NPs, the wavelength-dependent TPA cross section (δ) of the hybrid P-F8-DPSB NPs in the wavelength range of 750−850 nm was acquired with the results shown in Figure 2. Specifically, the hybrid NPs with diameter of ∼45 nm displayed δ value of 2.3×10^6 GM per nanoparticle upon 800 nm

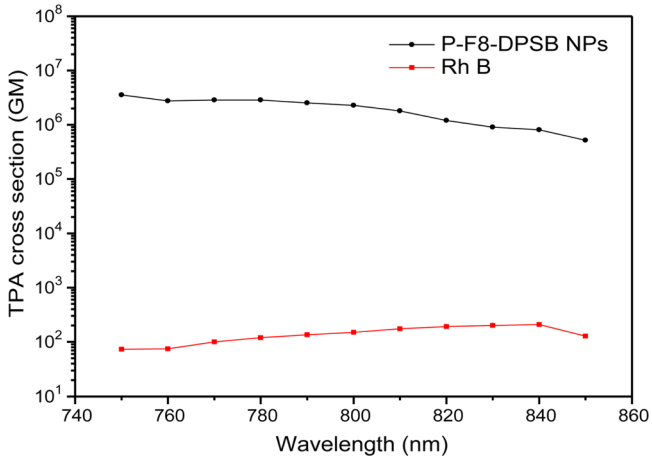

Figure 2. Plot of TPA cross sections of the hybrid P-F8-DPSB/DPA-PR-PDI NPs versus the excitation wavelength. For comparison, the wavelength-dependent δ of rhodamine B, a standard, was illustrated.

excitation with rhodamine B as the reference, which is much higher than that of other types of NPs reported previously.[19,30,35−37] Such high δ value, together with the high fluorescence quantum yield of the P-F8-DPSB in NPs, ∼45%, and their NIR fluorescence emission as discussed in the next section, suggests their great potential for TPA imaging.

Figure 3A displays the normalized UV−vis absorption and fluorescence emission spectra of the TPA polymer P-F8-DPSB and the NIR dye DPA-PR-PDI. It can be seen that P-F8-DPSB exhibits broad emission band in the range of 450−650 nm, while the NIR dye DPA-PR-PDI absorbs strongly in the range of 500−750 nm. Thus, the overlap of the emission band of P-F8-DPSB (donor) with the absorption band of DPA-PR-PDI (acceptor) enables an intercomponent energy transfer from the former to the latter in the hybrid NPs. As a result, two-photon excitation of P-F8-DPSB components eventually activates the emission of DPA-PR-PDI dye in the NIR region. Figure 3B displays the fluorescence emission spectra of the hybrid P-F8-DPSB/DPA-PR-PDI NPs with various polymer/dye ratios upon 800 nm excitation. It can be clearly seen that upon increasing the ratio of DPA-PR-PDI dye in the hybrid NPs, the NIR emission band centered at 730 nm attributable to the DPA-PR-PDI gradually augmented at the expense of the emission band originating from the P-F8-DPSB component. Specifically, in the case of hybrid NPs with ∼9.1% DPA-PR-PDI dye, fluorescence emission of the P-F8-DPSB component significantly attenuated and simultaneously the emission intensity centered at 730 nm displayed a 375-fold increase as compared to the emission features of NPs without DPA-PR-PDI. Additionally, energy transfer efficiency up to 90% from the donor to the acceptor in such case was determined. Such efficient energy transfer from TPA active component to the NIR-emitting dye, together with the super two-photon harvesting ability of the P-F8-DPSB component, is expected to impart the hybrid NPs with strong NIR fluorescence emission upon NIR two-photon excitation for biological imaging.

Figure 4 displays the fluorescence emission feature of the hybrid NPs with various ratio of NIR dye to TPA polymer. It can be seen that when the percentage of NIR dye increased up to 9.1%, the fluorescence intensity of NIR dye at 730 nm reached a

DOI: 10.1021/acsami.5b05150
ACS Appl. Mater. Interfaces 2015, 7, 20640−20648

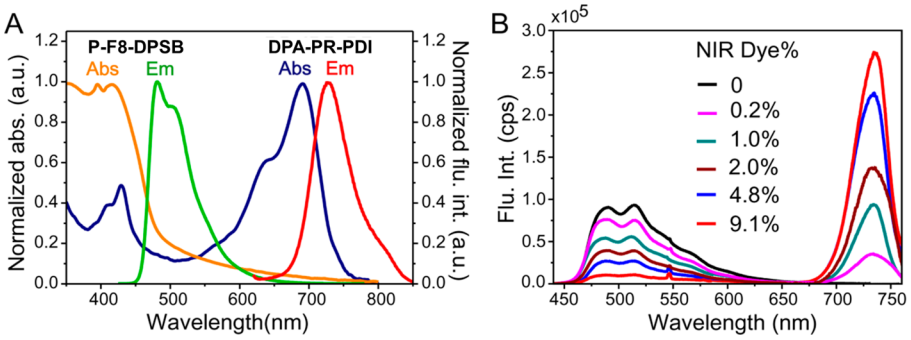

Figure 3. (A) Normalized absorption and fluorescence emission spectra of P-F8-DPSB polymer and DPA-PR-PDI in THF solution. (B) Fluorescence emission spectra of the hybrid P-F8-DPSB/DPA-PR-PDI NPs with various polymer/dye ratios upon 800 nm excitation.

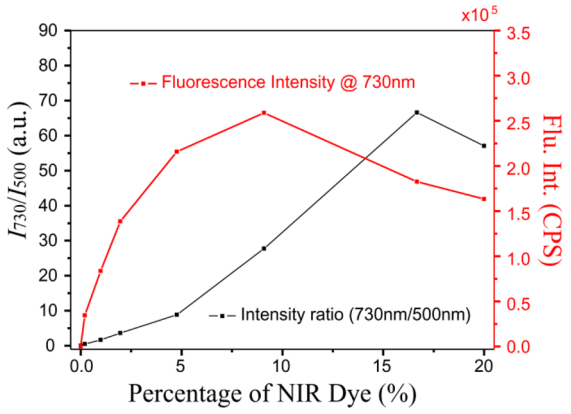

Figure 4. Two-photon excitation fluorescence intensity of P-F8-DPSB/DPA-PR-PDI NPs with various TPA/NIR dye ratios. λ_{ex} = 800 nm.

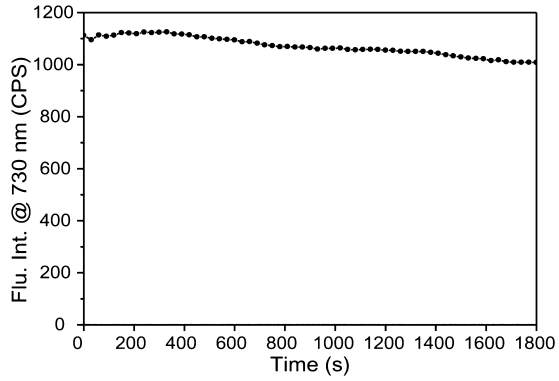

Figure 5. Evolution of the fluorescence intensity (at 730 nm) of the hybrid NPs encapsulated with FA-F127 under continuous illumination of 800 nm laser.

maximum and a further increase in the NIR dye percentage led to sharp decline in the intensity. It is noted that the fluorescence intensity ratio, I_{730}/I_{500}, displayed a maximum in the case of NPs with 16% NIR dye, which suggests the most efficient energy transfer from the donor to acceptor. However, the NIR fluorescence emission intensity in this case was much weaker than that of the NPs with 9.1% NIR dye, most probably a result of aggregation-induced fluorescence self-quenching of the NIR dye upon increasing the doping ratio.

As a typical nonlinear optical process in bioimaging, TPEF is inherently based on efficient two-photon excitation at a specific wavelength with the involvement of a resonance of the two-photon absorbing fluorescent agent.[10] It is worth noting that owing to the underlying resonant nature, TPEF probes are potentially susceptible to photobleaching or reduction in fluorescing ability upon continuous excitation. On the other hand, for application of probes in fluorescence-based imaging, photostability, or photobleaching resistance, is a critical measure, particularly for long-term imaging applications involving live cells and tissue.[26] To evaluate the photostability of the hybrid NPs in bioimaging experiment, aqueous dispersion sample with suspended hybrid NPs encapsulated with FA-F127 was spun on the coverslip to evenly distribute the NPs; the coverslip with NPs was then placed on the sample stage for bioimaging and the fluorescence intensity at 730 nm of the sample was acquired every 30 s upon continuous illumination of an 800 nm pulse laser. Specifically, the illumination power of the pulse laser was set as the same as that used in the typical cell fluorescence imaging. As shown in Figure 5, upon 0.5 h continuous laser illumination, ~9% fluorescence intensity loss of NPs was found, suggesting the perfect photostability of the hybrid NPs in the present work for TPEF-based imaging.

In practical fluorescence imaging applications involving live cells and tissue, one of the key litmus test for fluorescent probes is whether they are capable of circumventing the impediment of penetration depth of the incoming (excitation) light and the attenuation of the outgoing (emission) light owing to absorption and light scattering caused by cellular structures and tissues. To evaluate the performance of P-F8-DPSB/DPA-PR-PDI NPs in deep tissue fluorescence imaging, the imaging depth of two types of P-F8-DPSB-containing fluorescent NPs was investigated with the results shown in Figure 6. The left column displays the fluorescence imaging results using P-F8-DPSB-based NPs as probes and 405 nm light as the excitation source by collecting the fluorescence signal in the range of 450−550 nm. The medium and the right columns show the fluorescence imaging results using hybrid P-F8-DPSB/DPA-PR-PDI NPs as probes by collecting the fluorescence signal in the range of 650−730 nm with 405 and 800 nm light in the case of medium and right columns, respectively, as the excitation sources. Specifically, a 10× objective lens with long working distance was used in the imaging experiments with various mock tissue depths and the laser powers were adjusted for acquiring fluorescence images with roughly similar brightness in the cases of samples without mock tissue (the top images in three columns). It can be seen that in the cases of imaging by collecting emission signal in the range of 450−550 nm upon excitation of 405 nm light, mock tissue with 300-μm thickness significantly attenuated the collected fluorescence signal, which is attributable to the serious absorption and light scattering caused by the mock tissue to excitation and emission light, both in the visible range. In

DOI: 10.1021/acsami.5b05150
ACS Appl. Mater. Interfaces 2015, 7, 20640−20648

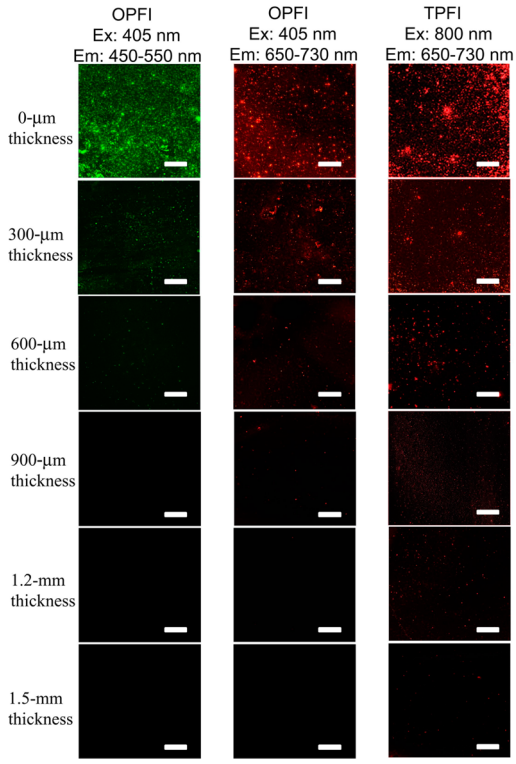

Figure 6. Evaluation of the penetration ability of hybrid fluorescent NPs for fluorescence imaging under different imaging modes. The scale bar refers to 100 μm.

contrast, in the cases of imaging by collecting emission signal in the range of 650−730 nm upon excitation of 405 nm light, the attenuation effect that the mock tissue exerted on the collected fluorescence signal was obviously alleviated. Specifically, in the case of sample with 900-μm thickness of mock tissue, fluorescence signal from single nanoparticle can be clearly observed. A larger imaging depth was observed in the case of imaging by collecting emission signal in the range of 650−730 nm upon excitation of 800 nm light, which demonstrates clear fluorescence image of NPs even with the challenge of mock tissue with thickness of 1200 μm. Unequivocally, such excellent performance of the fluorescent probes in deep-tissue imaging observed in the NIR-input-NIR-output mode is attributable to the strong penetration ability of excitation and emission light in the NIR region. It is important to note that for NIR fluorescence imaging results shown in Figure 6, only fluorescence signals in the range of 650−730 nm were collected while those in the range of 730−800 nm lost due to the limit of instrument used in the present work, as illustrated in Figure 3. Therefore, using instrument with optimum capacity regarding to the energy range of collected photon is expected to roughly double the amount of NIR photons collected from the hybrid NPs and consequently enables the NPs with larger penetration depth in fluorescence imaging experiment of thick samples.

Taking the growing safety concerns about the use of artificial NPs in biological systems, we evaluated the cytotoxicity of the hybrid NPs themselves. As shown in Figure 7, less than 5% decrease in the cell viability was observed when Hela cells were treated with the hybrid NPs with concentration of 10 μg/mL. Although the cell viability displayed gradual decrease upon increasing the concentration of NPs, more than 81% cells survived in the case of cells incubation with the NPs with

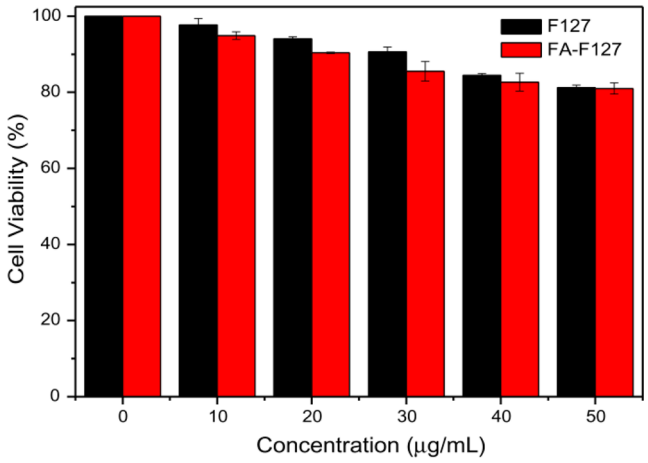

Figure 7. Cell viability assays of HeLa cells treated with P-F8-DPSB/DPA-PR-PDI NPs with encapsulation of F127 and FA-F127 for 12 h.

concentration up to 50 μg/mL for 12 h. It deserves mentioning that the concentration of NPs used in cell imaging in the present work was ∼8 μg/mL. Thus, the hybrid NPs developed herein possess good biocompatibility for biological applications.

To validate the application of the hybrid NPs for TPEF biological imaging, TPEF images of the NPs residing in HeLa cancer cells were acquired. For a typical imaging protocol, HeLa cancer cells were incubated with 8 μg/mL P-F8-DPSB/DPA-PR-PDI NPs with encapsulation of F127 and FA-F127, respectively, for 2 h. After incubation, the cells were immobilized by 4% formaldehyde solution following by PBS buffer rinse to remove any residual fluorescent probes. Cells were subsequently imaged using 800 nm light to excite the fluorescence images. Figure 8 displays the representative cell fluorescence images with internalized hybrid NPs. It can be seen that the hybrid NPs were phagocytized by HeLa cancer cells after incubation and the bright fluorescent spots clearly light up cell organelles. Additionally, cells after incubation with the hybrid fluorescent NPs with encapsulation of FA-F127 fluoresce intensely with their nuclear membrane area clearly illuminated (Figure 8C). In contrast, the cells after incubation with F127-encapsulated hybrid NPs without the decoration of FA components displayed relatively weak fluorescence and faint cellular contour (Figure 8A). It is known that FA component preferentially binds to the FA receptor that is highly expressed on the surfaces of cancer cells, which is anticipated to facilitate the receptor-mediated endocytosis of the exogenous nanoparticle. Therefore, the observed discrepancy in the fluorescence brightness in cells is attributable to the targeting effect of FA component decorated on the surface of NPs.

The litmus test for the as-prepared fluorescent probes is whether they are capable of defying the impediment that the thick tissue brings out in biological imaging. Figure 8 B and D display the fluorescence images of HeLa cells with internalized F127-encapsuled and FA-F127-encapsuled hybrid NPs, respectively, in the presence of mock tissue with 900-μm thickness. As compared to their counterpart fluorescence images acquired in the absence of mock tissue as shown in Figure 8 A and C, signals in Figure 8 B and D were obviously attenuated due to the scattering effect that the mock tissue brings out. However, even in the case of imaging with the challenge of mock tissue with thickness up to 900 μm, the bright fluorescence of the target NPs in the cells can be clearly observed, particularly for FA-F127-encapsuled hybrid NPs. These preliminary fluorescence imaging

DOI: 10.1021/acsami.5b05150
ACS Appl. Mater. Interfaces 2015, 7, 20640−20648

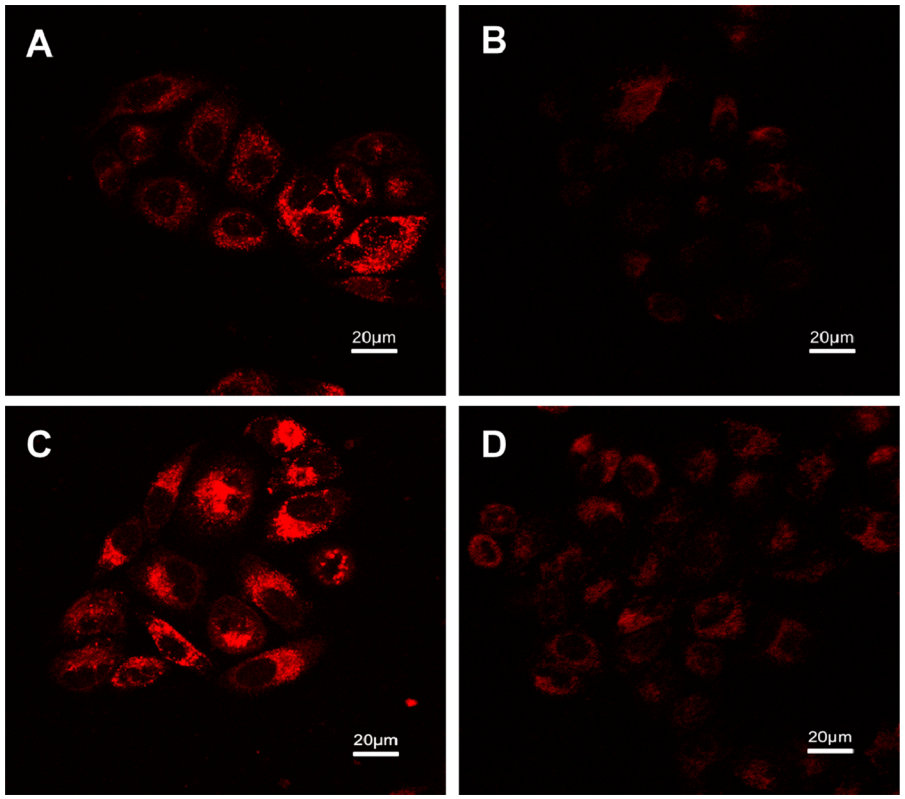

Figure 8. TPEF-based penetration imaging of Hela cells after incubation with 8 μg/mL of hybrid NPs acquired by collecting the fluorescence signal in the range of 650−730 nm. A and B: F127-encapsuled NPs, mock tissue thickness of 0- and 900-μm, respectively. C and D: FA-F127-encapsuled NPs, mock tissue thickness of 0- and 900-μm, respectively.

results voted our hybrid NPs as a type of effective probes for TPEF-based biological imaging. It deserves mentioning that, due to the limit of instrument used in the present work, the fluorescence imaging results shown in Figure 8 were acquired on the basis of losing approximately half of the photon that the NPs emit. Thus, cell fluorescence imaging with improved signal-to-noise ratio can be anticipated by using instrument with optimum capacity regarding to the energy range of collected photon.

CONCLUSIONS

In this Research Article, we describe the synthesis, properties, and preliminary intracellular fluorescence imaging application of a new type of hybrid NPs characterized by NIR-fluorescence emission upon TPA-based excitation of pulse laser with wavelength in NIR region. Such NIR-input-NIR-output fluorescence feature is based on the efficient FRET process from conjugated polymer with excellent TPA property, the donor, to fluorophore with NIR-fluorescence emission feature, the acceptor. As a desirable property of fluorescent probe for biological application, such TPEF-based NIR-input-NIR-output feature intrinsically imparts the hybrid NPs with superb ability for imaging deep-seated target with penetration depth up to 1200 μm. The preliminary fluorescence bioimaging experiments have revealed the facile cellular ingestion and biocompatibility of the as-prepared probes, and the TPEF penetration imaging experiments validated their practicability for tissue imaging with thickness up to millimeter scale. In spite of considerable amount of effort devoted to the development of fluorescent probes for multiphoton fluorescence imaging, previous paradigms where a conjugated polymer based fluorescent probe with TPA-based excitation and fluorescence emission both in NIR region have been scarcely reported. The above-mentioned figure of merits of the hybrid NPs developed in the present work is indicative of the potential of these fluorescent NPs for bioimaging of scattering samples, such as thick tissue.

AUTHOR INFORMATION

Corresponding Authors

*E-mail: msfhuang@scut.edu.cn.
*E-mail: yszhao@iccas.ac.cn.
*E-mail: zytian@ucas.ac.cn.

Author Contributions

Y.L. and P.L. contributed equally to this work.

Notes

The authors declare no competing financial interest.

ACKNOWLEDGMENTS

This work was financially supported by the National Natural Science Foundation of China (grant nos. 21173262, 21373218, and 91233107) and the "Hundred-Talent Program" of CAS to Z.T.

REFERENCES

(1) Evanko, D. Focus on Fluorescence Imaging. *Nat. Methods* **2005**, *2*, 901.
(2) Pepperkok, R.; Ellenberg, J. High-Throughput Fluorescence Microscopy for Systems Biology. *Nat. Rev. Mol. Cell Biol.* **2006**, *7*, 690−696.
(3) Yildiz, A.; Forkey, J. N.; McKinney, S. A.; Ha, T.; Goldman, Y. E.; Selvin, P. R.; Myosin, V. Walks Hand-Over-Hand: Single Fluorophore Imaging with 1.5-nm Localization. *Science* **2003**, *300*, 2061−2065.

DOI: 10.1021/acsami.5b05150
ACS Appl. Mater. Interfaces 2015, 7, 20640−20648

(4) Neto, B. A. D.; Carvalho, P. H. P. R.; Correa, J. R. Benzothiadiazole Derivatives as Fluorescence Imaging Probes: Beyond Classical Scaffolds. *Acc. Chem. Res.* **2015**, *48*, 1560−1569.
(5) Mason, W. T. *Fluorescent and Luminescent Probes for Biological Activity*, 2nd ed.; Academic Press: London, 1999.
(6) Lakowicz, J. R. *Principles of Fluorescence Spectroscopy*, 3rd ed.; Springer: New York, 2006.
(7) Marti, A. A.; Jockusch, S.; Stevens, N.; Ju, J. Y.; Turro, N. J. Fluorescent Hybridization Probes for Sensitive and Selective DNA and RNA Detection. *Acc. Chem. Res.* **2007**, *40*, 402−409.
(8) Giepmans, B. N. G.; Adams, S. R.; Ellisman, M. H.; Tsien, R. Y. The Fluorescent Toolbox for Assessing Protein Location and Function. *Science* **2006**, *312*, 217−224.
(9) Gu, M.; Gan, X. S.; Kisteman, A.; Xu, M. G. Comparison of Penetration Depth between Two-Photon Excitation and Single-photon Excitation in Imaging through Turbid Tissue Media. *Appl. Phys. Lett.* **2000**, *77*, 1551−1553.
(10) Ohulchanskyy, T. Y.; Pliss, A. M.; Prasad, P. N. Biophotonics: Harnessing Light for Biology and Medicine. *Nato. Sci. Peace Sec. B* **2011**, 3−17.
(11) Maestro, L. M.; Ramirez-Hernandez, J. E.; Bogdan, N.; Capobianco, J. A.; Vetrone, F.; Sole, J. G.; Jaque, D. Deep Tissue Bio-Imaging Using Two-photon Excited CdTe Fluorescent Quantum Dots Working within the Biological Window. *Nanoscale* **2012**, *4*, 298−302.
(12) Crosignani, V.; Dvornikov, A.; Aguilar, J. S.; Stringari, C.; Edwards, R.; Mantulin, W. W.; Gratton, E. Deep Tissue Fluorescence Imaging and In Vivo Biological Applications. *J. Biomed. Opt.* **2012**, *17*, 116023.
(13) Liu, Q.; Guo, B. D.; Rao, Z. Y.; Zhang, B. H.; Gong, J. R. Strong Two-Photon-Induced Fluorescence from Photostable, Biocompatible Nitrogen-Doped Graphene Quantum Dots for Cellular and Deep-Tissue Imaging. *Nano Lett.* **2013**, *13*, 2436−2441.
(14) Yu, J. H.; Kwon, S. H.; Petrasek, Z.; Park, O. K.; Jun, S. W.; Shin, K.; Choi, M.; Park, Y. I.; Park, K.; Na, H. B.; Lee, N.; Lee, D. W.; Kim, J. H.; Schwille, P.; Hyeon, T. High-Resolution Three-Photon Biomedical Imaging Using Doped ZnS Nanocrystals. *Nat. Mater.* **2013**, *12*, 359−366.
(15) Langer, G.; Bouchal, K. D.; Grun, H.; Burgholzer, P.; Berer, T. Two-photon Absorption-induced Photoacoustic Imaging of Rhodamine B Dyed Polyethylene Spheres Using a Femtosecond Laser. *Opt. Express* **2013**, *21*, 22410−22422.
(16) Lim, C. S.; Cho, B. R. Two-Photon Probes for Biomedical Applications. *Bmb. Rep.* **2013**, *46*, 188−194.
(17) Crosignani, V.; Dvornikov, A.; Gratton, E. Ultra-deep Imaging of Turbid Samples by Enhanced Photon Harvesting. *Proc. SPIE* **2013**, *8588*, 858810.
(18) Crosignani, V.; Jahid, S.; Dvornikov, A.; Gratton, E. Deep Tissue Imaging by Enhanced Photon Collection. *J. Innovative Opt. Health Sci.* **2014**, *7*, 1450034.
(19) Geng, J. L.; Goh, C. C.; Tomczak, N.; Liu, J.; Liu, R. R.; Ma, L.; Ng, L. G.; Gurzadyan, G. G.; Liu, B. Micelle/Silica Co-protected Conjugated Polymer NPs for Two-Photon Excited Brain Vascular Imaging. *Chem. Mater.* **2014**, *26*, 1874−1880.
(20) Stanciu, S. G.; Xu, S. Y.; Peng, Q. W.; Yan, J.; Stanciu, G. A.; Welsch, R. E.; So, P. T. C.; Csucs, G.; Yu, H. Experimenting Liver Fibrosis Diagnostic by Two Photon Excitation Microscopy and Bag-of-Features Image Classification. *Sci. Rep.* **2014**, *4*, 4636.
(21) Yi, M.; Yang, S.; Peng, Z. Y.; Liu, C. H.; Li, J. S.; Zhong, W. W.; Yang, R. H.; Tan, W. H. Two-Photon Graphene Oxide/Aptamer Nanosensing Conjugate for In Vitro or In Vivo Molecular Probing. *Anal. Chem.* **2014**, *86*, 3548−3554.
(22) Zhang, H.; Fan, J. L.; Wang, K.; Li, J.; Wang, C. X.; Nie, Y. M.; Jiang, T.; Mu, H. Y.; Peng, X. J.; Jiang, K. Highly Sensitive Naphthalene-Based Two-Photon Fluorescent Probe for in Situ Real-Time Bioimaging of Ultratrace Cyclooxygenase-2 in Living Biosystems. *Anal. Chem.* **2014**, *86*, 9131−9138.
(23) Hong, G. S.; Zou, Y. P.; Antaris, A. L.; Diao, S.; Wu, D.; Cheng, K.; Zhang, X. D.; Chen, C. X.; Liu, B.; He, Y. H.; Wu, J. Z.; Yuan, J.; Zhang, B.; Tao, Z. M.; Fukunaga, C.; Dai, H. J. Ultrafast Fluorescence Imaging In Vivo with Conjugated Polymer Fluorophores in the Second Near-Infrared Window. *Nat. Commun.* **2014**, *5*, 4206.
(24) Tao, Z. M.; Hong, G. S.; Shinji, C.; Chen, C. X.; Diao, S.; Antaris, A. L.; Zhang, B.; Zou, Y. P.; Dai, H. J. Biological Imaging Using NPs of Small Organic Molecules with Fluorescence Emission at Wavelengths Longer than 1000 nm. *Angew. Chem., Int. Ed.* **2013**, *52*, 13002−13006.
(25) Jin, Y. H.; Ye, F. M.; Zeigler, M.; Wu, C. F.; Chiu, D. T. Near-Infrared Fluorescent Dye-Doped Semiconducting Polymer Dots. *ACS Nano* **2011**, *5*, 1468−1475.
(26) Liu, P.; Li, S.; Jin, Y. C.; Qian, L. H.; Gao, N. Y.; Yao, S. Q.; Huang, F.; Xu, Q. H.; Cao, Y. Red-Emitting DPSB-Based Conjugated Polymer NPs with High Two-Photon Brightness for Cell Membrane Imaging. *ACS Appl. Mater. Interfaces* **2015**, *7*, 6754−6763.
(27) Hou, Q.; Xu, Y.; Yang, W.; Yuan, M.; Peng, J.; Cao, Y. Novel Red-Emitting Fluorene-Based Copolymers. *J. Mater. Chem.* **2002**, *12*, 2887−2892.
(28) Shibano, Y.; Umeyama, T.; Matano, Y.; Imahori, H. Electron-Donating Perylenetetracarboxylic Acids for Dye-Sensitized Solar Cells. *Org. Lett.* **2007**, *9*, 1971−1974.
(29) Ling, D.; Xia, H.; Park, W.; Hackett, M. J.; Song, C.; Na, K.; Hui, K. M.; Hyeon, T. pH-Sensitive Nanoformulated Triptolide as a Targeted Therapeutic Strategy for Hepatocellular Carcinoma. *ACS Nano* **2014**, *8*, 8027−8039.
(30) Xu, Z. Z.; Liao, Q.; Wu, Y. S.; Ren, W. L.; Li, W.; Liu, L. B.; Wang, S.; Gu, Z. J.; Zhang, H. L.; Fu, H. B. Water-Miscible Organic J-aggregate NPs as Efficient Two-Photon Fluorescent Nano-Probes for Bio-Imaging. *J. Mater. Chem.* **2012**, *22*, 17737−17743.
(31) Lv, P. P.; Ma, Y. F.; Yu, R.; Yue, H.; Ni, D. Z.; Wei, W.; Ma, G. H. Targeted Delivery of Insoluble Cargo (Paclitaxel) by PEGylated Chitosan Nanoparticles Grafted with Arg-Gly-Asp (RGD). *Mol. Pharmaceutics* **2012**, *9*, 1736−1747.
(32) Wu, C. F.; Szymanski, C.; Cain, Z.; McNeill, J. Conjugated Polymer Dots for Multiphoton Fluorescence Imaging. *J. Am. Chem. Soc.* **2007**, *129*, 12904−12905.
(33) Wu, C. F.; Zheng, Y. L.; Szymanski, C.; McNeill, J. D. Energy Transfer in a Nanoscale Multichromophoric System: Fluorescent Dye-Doped Conjugated Polymer NPs. *J. Phys. Chem. C* **2008**, *112*, 1772−1781.
(34) Tian, Z. Y.; Yu, J. B.; Wang, X. L.; Groff, L. C.; Grimland, J. L.; McNeill, J. D. Conjugated Polymer NPs Incorporating Antifade Additives for Improved Brightness and Photostability. *J. Phys. Chem. B* **2013**, *117*, 4517−4520.
(35) Li, K.; Jiang, Y. H.; Ding, D.; Zhang, X. H.; Liu, Y. T.; Hua, J. L.; Feng, S. S.; Liu, B. Folic Acid-Functionalized Two-Photon Absorbing NPs for Targeted MCF-7 Cancer Cell Imaging. *Chem. Commun.* **2011**, *47*, 7323−7325.
(36) Qian, J.; Zhu, Z. F.; Qin, A. J.; Qin, W.; Chu, L. L.; Cai, F. H.; Zhang, H. Q.; Wu, Q.; Hu, R. R.; Tang, B. Z.; He, S. L. High-Order Non-Linear Optical Effects in Organic Luminogens with Aggregation-Induced Emission. *Adv. Mater.* **2015**, *27*, 2332−2339.
(37) Aparicio-Ixta, L.; Ramos-Ortiz, G.; Pichardo-Molina, J. L.; Maldonado, J. L.; Rodriguez, M.; Tellez-Lopez, V. M.; Martinez-Fong, D.; Zolotukhin, M. G.; Fomine, S.; Meneses-Nava, M. A.; Barbosa-Garcia, O. Two-Photon Excited Fluorescence of Silica NPs Loaded with a Fluorene-Based Monomer and Its Cross-Conjugated Polymer: Their Application to Cell Imaging. *Nanoscale* **2012**, *4*, 7751−7759.

DOI: 10.1021/acsami.5b05150
ACS Appl. Mater. Interfaces 2015, 7, 20640−20648